Increasing Liquid State Machine Performance with Edge-of-Chaos Dynamics Organized by Astrocyte-modulated Plasticity

Anonymous Author(s)
Affiliation
Address
email

Abstract

The liquid state machine (LSM) combines low training complexity and biological plausibility, which has made it an attractive machine learning framework for edge and neuromorphic computing paradigms. Originally proposed as a model of brain computation, the LSM tunes its internal weights without backpropagation of gradients, which results in lower performance compared to multi-layer neural networks. Recent findings in neuroscience suggest that astrocytes, a long-neglected non-neuronal brain cell, modulate synaptic plasticity and brain dynamics, tuning brain networks into the computationally optimal critical phase transition between order and chaos. Inspired by this disruptive understanding of how brain networks self-tune, we propose the neuron-astrocyte liquid state machine (NALSM) that addresses under-performance through self-organized critical dynamics. Similar to its biological counterpart, the astrocyte model integrates neuronal activity and provides global feedback to spike-timing-dependent plasticity (STDP), which self-organizes NALSM dynamics at the edge-of-chaos. We demonstrate that NALSM achieves state-of-the-art accuracy versus comparable LSM methods, without the need for data-specific hand-tuning. With a top accuracy of 97.61% on MNIST and 97.51% on N-MNIST, NALSM achieved comparable performance to current fully-connected multi-layer spiking neural networks trained via backpropagation. Our findings suggest that the further development of brain-inspired machine learning methods has the potential to reach the performance of deep learning, with the added benefits of supporting robust and energy-efficient neuromorphic computing on the edge.

1 Introduction

With the recent rise of neuromorphic [1–4] and edge computing [5, 6], the liquid state machine (LSM) learning framework [7] has become an attractive alternative [8–11] to deep neural networks owing to its compatibility with energy-efficient neuromorphic hardware [12–14] and inherently low training complexity. Originally proposed as a biologically plausible model of learning, LSMs avoid training via backpropagation by using a sparse, recurrent, spiking neural network (liquid) with fixed synaptic connection weights to project inputs into a high dimensional space from which a single neural layer can learn the correct outputs. Yet, these advantages over deep networks come at the expense of 1) sub-par accuracy and 2) extensive data-specific hand-tuning of liquid weights. Interestingly, these two limitations have been targeted by several studies that tackle one [15, 16] or the other [17, 18], but not both. This has limited the widespread use of LSMs in real-world applications [8]. In that sense, there is an unmet need for a unified, brain-inspired approach that is directly applicable to the emerging neuromorphic and edge computing technologies, facilitating them to go mainstream.

Submitted to 35th Conference on Neural Information Processing Systems (NeurIPS 2021). Do not distribute.

As a general heuristic, LSM accuracy is maximized when LSM dynamics are positioned near a critical phase transition [19–21] separating: 1) order, the sub-critical phase where network activity decays, and 2) chaos, the super-critical phase where network activity gets exponentially amplified. Strikingly, brain networks have also been found to operate near the edge-of-chaos [22–24]. Current methods organize LSMs at criticality by adding forward and backward communication channels on top of the liquid [15, 16]. This significantly increases training complexity and violates the LSM's brain-inspired self-organization principles. For example, these methods lack local plasticity rules that are widely observed in the brain and considered a key component for both biological [25] and neuromorphic learning [3, 2, 4]. A particular local learning rule, spike-timing-dependent plasticity (STDP), is known to improve LSM accuracy [17, 18]. Yet, current methods of incorporating STDP into LSMs further exacerbate the limitations of data-specific hand-tuning as they require additional mechanisms to compensate for the STDP-imposed saturation of synaptic weights [17, 26–29]. This signifies the scarcity of LSM tuning methods that are both computationally efficient and data-independent.

A long-neglected non-neuronal cell in the brain, astrocytes, is now known to play key roles in modulating brain networks [30–35], from modifying synaptic plasticity [36–38] to facilitating switching between cognitive states [39–42] that have been linked to a narrow spectrum of dynamics around the critical phase transition [43–47]. The mechanisms that astrocytes use to modulate neurons include the integration of the activity of thousands of synapses into a slow intracellular continuous signal that feeds back to neurons by affecting their synaptic plasticity [48–51, 38]. The unique spatio-temporal attributes [52, 53] identified in astrocytes align well with the brain's remarkable ability to self-organize its massive and highly recursive networks near the edge-of-chaos. That is why astrocytes present a fascinating possibility of forming a unified feedback modulation mechanism required to improve baseline LSM accuracy while eliminating data-specific hand-tuning.

Here, we propose the neuron-astrocyte liquid state machine (NALSM), where a biologically plausible astrocyte model organizes liquid dynamics at the edge-of-chaos by modulating STDP weight changes. We show that NALSM combines the computational benefits of both STDP and edge-of-chaos dynamics by demonstrating its accuracy advantage compared to other LSM methods on two datasets: 1) MNIST [54], and 2) N-MNIST [55]. We demonstrate that, similar to its biological counterpart that handles new and unstructured information with robustness and versatility, NALSM maintains the state-of-the-art LSM performance without re-tuning training parameters for each dataset. We also show that a NALSM with a large enough liquid can attain comparable accuracy to fully-connected multi-layer spiking neural networks trained via backpropagation. Our results suggest that the under-performance and high training difficulty of current neuromorphic methods can be addressed by harvesting neuroscience knowledge and further translating biological principles to computational mechanisms.

2 Methods

2.1 The neuron-astrocyte liquid state machine

To construct the NALSM, we started with a baseline LSM model consisting of 2 layers: 1) a spiking liquid, and 2) a linear output layer. Next, we added STDP to the LSM liquid, forming the LSM+STDP model. We developed a biologically faithful leaky-integrate-and-modulate (LIM) astrocyte model, which we embedded in the LSM+STDP liquid, to form the NALSM. The process is formalized below.

LSM Model We implemented the baseline LSM as a 3-dimensional neural network (liquid) consisting of $1,000$ neurons surrounded by 1-dimensional layers of input and output neurons. Number of input neurons was 784 and $2,312$ for MNIST and N-MNIST, respectively (See Appendix A.1). We used the leaky-integrate-and-fire (LIF) model [3] for input and liquid neurons, modeled as:

$$\frac{dv_i}{dt} = -\frac{1}{\tau_v} v_i(t) + u_i(t) - \theta_i \sigma_i(t) \tag{1}$$

$$u_i(t) = \sum_{j \neq i} w_{ij} (\alpha_u * \sigma_j)(t) + b_i \tag{2}$$

where v_i is the membrane potential and u_i is the synaptic response current of neuron i, θ_i is the membrane potential threshold, $\sigma_i(t) = \sum_k \delta(t - t_i^k)$ is the spike train of neuron i with t_i^k being the time of the k-th spike, $w_{i,j}$ is the weight connecting neuron j to i, b_i is the bias of neuron

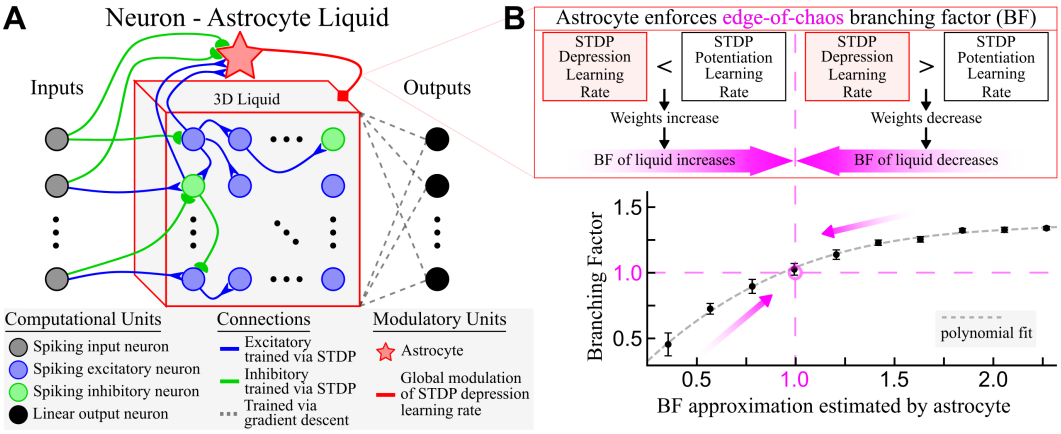

Figure 1: **NALSM architecture and astrocyte modulation of liquid dynamics.** (**A**) The neuron-astrocyte liquid was modeled as a 3-dimensional network of excitatory and inhibitory spiking neurons connected with sparse, recurrent connections with spike-timing-dependent plasticity (STDP). Input neurons projected excitatory and inhibitory connections to the liquid. Receiving each liquid neuron's spike count per input sample, a dense linear output layer was trained via gradient descent to classify inputs. (**B**) To organize edge-of-chaos liquid dynamics, an astrocyte integrated input and liquid neuron activity and, in turn, set the global STDP depression learning rate. Data points are binned averages over 'BF approximation' metric. Error bars are standard deviation. See Appendix A.9 for polynomial fits.

i, and $\alpha_u(t) = \tau_u^{-1} \exp(-t/\tau_u) H(t)$ is the synaptic filter with H(t) being the unit step function (See Appendix A.3). All LIF neurons had a 2 ms absolute refractory period. Liquid neurons were excitatory and inhibitory with $80\%/20\%$ ratio. Input neurons did not have an excitatory/inhibitory distinction and had random excitatory and inhibitory connections to liquid neurons. From here on, we will refer to connections between input neurons and liquid neurons as IL connections, inter-liquid connections as LL, and liquid to output connections as LO. In line with [7], we created LL connections using probabilities based on Euclidean distance, $D(i, j)$, between any two neurons i, j:

$$P(i, j) = C \cdot exp\left(-\left(\frac{D(i, j)}{\lambda}\right)^2\right) \tag{3}$$

with closer neurons having higher connection probability (See Appendix A.4). Density of IL connections was 15%. The output layer was a dense layer of 10 linear neurons.

LSM+STDP Model We added unsupervised, local learning to the LSM model by letting STDP change all LL and IL connections [56], modeled as:

$$\frac{dw}{dt} = A_+ T_{pre} \sum_o \delta(t - t^o_{post}) - A_- T_{post} \sum_i \delta(t - t^i_{pre}) \tag{4}$$

where $A_+ = A_- = 0.15$ are the potentiation/depression learning rates and T_{pre}/T_{post} are the pre/post-synaptic trace variables modeled as,

$$\tau^*_+ \frac{dT_{pre}}{dt} = -T_{pre} + a_+ \sum_i \delta(t - t^i_{pre}) \tag{5}$$

$$\tau^*_- \frac{dT_{post}}{dt} = -T_{post} + a_- \sum_o \delta(t - t^o_{post}) \tag{6}$$

where $a_+ = a_- = 0.1$ are the discrete contributions of each spike to the trace variable, $\tau^*_+ = \tau^*_- = 10$ ms are the decay time constants, t^i_{pre} and t^o_{post} are the times of the pre-synaptic and post-synaptic spikes, respectively. We constrained connection weights to: 1) IL: $[-3, 3]$, 2) excitatory LL: $[0, 3]$, and 3) inhibitory LL: $[-3, 0]$. We used the same STDP parameters for all models and experiments.

The LIM Astrocyte Model We developed the astrocyte model as a leaky integrator with a continuous output value A_{-}^{astro}, expressed as:

$$\tau_{asto}\frac{dA_{-}^{astro}}{dt} = -A_{-}^{astro} + w_{astro}\sum_{i\in N_{liq}}\delta(t-t_i) - w_{astro}\sum_{j\in N_{inp}}\delta(t-t_j) + b_{astro} \quad (7)$$

where $A_{-}^{astro} \rightarrow A_{-}$ directly sets the STDP depression learning rate, $b_{astro} = A_{+}$ adjusts the astrocyte output to the fixed STDP potentiation learning rate, N_{liq} and N_{inp} are the sets of liquid and input neurons, respectively, and w_{astro} sets astrocytic responsiveness to network activity (See Appendix A.5). Ignoring the decay and bias terms, the astrocyte model computes the difference in the number of spikes produced by liquid neurons and input neurons. Functionally, this is equivalent to computing the ratio of spikes emitted by the liquid over the input neurons:

$$BF_{proxy}(t) = \frac{\sum_{i\in N_{liq}}\delta(t-t_i)}{\sum_{j\in N_{inp}}\delta(t-t_j)} \quad (8)$$

Specifically, when the liquid produces more spikes than the input neurons, their difference is positive which translates to $BF_{proxy} > 1.0$, and vice versa. This approach to measure liquid dynamics is a network level approximation of the branching factor, σ_{BF}, which is normally evaluated for each neuron (See 2.3.1). We confirmed that $BF_{proxy} = 1.0$ aligned with the critical branching factor, $\sigma_{BF} = 1.0$ (Fig. 1 B). Hence, as dynamics become progressively chaotic ($\sigma_{BF} > 1.0$), BF_{proxy} becomes greater than 1, which causes the LIM astrocyte to increase STDP depression learning rate above the fixed STDP potentiation learning rate ($A_{-}^{astro} \rightarrow A_{-} > A_{+}$). This causes STDP to decrease the average weight of LL and IL connections, which decreases number of spikes produced by liquid and makes dynamics less chaotic (Fig. 1 B). The reverse occurs as dynamics become progressively ordered. As a result of astrocyte modulation, liquid dynamics oscillated between order and chaos until eventual stabilization at the critical branching factor (See Appendix A.5).

NALSM Model We completed NALSM by adding the LIM astrocyte to the LSM+STDP model's liquid (Fig. 1 A). As described above, the LIM astrocyte integrated activity from input and liquid neurons, and continuously controlled the STDP depression learning rate.

2.2 Training

Model training was done in 3 steps: 1) initialization of IL and LL liquid connections, 2) passing all data through the liquid resulting in liquid neuron spike counts, and 3) training the output layer on the spike counts. The steps are further detailed below.

2.2.1 Liquid initialization

LSM We initialized all IL and LL connections with a constant weight, maintaining originally defined connection signs. Weights were constant during spike count collection.

LSM+STDP We initialized IL and LL connections with STDP by consecutively presenting all the training images to the liquid. Starting with initially maximal connections, $3(-3)$ for excitatory(inhibitory) connections, we let STDP continuously adjusted weights while presenting the liquid with a randomly ordered series of MNIST training image snapshots, each lasting $20\ ms$. For N-MNIST, we randomly sampled each $20\ ms$ snapshot from the $0 - 250\ ms$ range, as a way to account for the variability in the temporal dimension (See 2.3). In each case, we used a total of $50,000$ snapshots, each corresponding to a unique training image. We used STDP only for weight initialization. Initialized weights were fixed during spike count collection.

NALSM We used the LSM+STDP weight initialization process with the exception of added STDP modulation by the LIM astrocyte (See 7). We used this set of initialized weights as the starting point for each sample in the spike counting phase, during which astrocyte modulated STDP continued to adjust synaptic weights. For each sample, parameters A_{+} from (4) and b_{astro} from (7) were both initialized to 0.15 and decayed at a rate of 0.99 for the duration of sample input.

2.2.2 Output layer training

We assembled spike counts by presenting each sample image to the liquid for $250\ ms$ and counting the number of spikes emitted by each liquid neuron for the full duration of input. We used Adam optimizer to batch train the output layer on spike count vectors by minimizing the cross entropy loss with L2-regularization,

$$\mathcal{L}(y_i, \hat{y}) = -\frac{1}{m}\sum_{i=1}^{m} y_i log(\hat{y}_i) + (1 - y_i) log(1 - \hat{y}_i) + \frac{\lambda_{reg}}{2m}||W_{out}||_F^2 \tag{9}$$

where $m = 250$ is the batch size, W_{out} is the output layer weight matrix, $\lambda_{reg} = 5 \times 10^{-10}$ is the regularization hyperparameter, y_i and $\hat{y}_i$ are the normalized vectors denoting the predicted label and the target label, respectively. Prior to training, we initialized output layer weights/biases to 0.0, and the learning rate to 0.1. We trained the output layer until validation accuracy peaked (up to a maximum of $5,000$ epochs), at which point we evaluated model test accuracy.

2.3 Experiments

We performed all experiments on MNIST and N-MNIST datasets (See A.1). Using 10 randomly generated networks for each dataset, we trained 1) the baseline LSM model, 2) the LSM+STDP model, 3) the NALSM model (See 2.1), and 4) the LSM+AP-STDP model, a method for incorporating STDP in the LSM liquid [17] (See Appendix A.6). First, we evaluated LSM model accuracy with respect to liquid weight, which ranged in $0.4 - 1.2$ for MNIST and $0.8 - 1.35$ for N-MNIST. We used a random seed for each training session. Next, we evaluated corresponding network dynamics of each network/weight combination by measuring the liquid's branching factor on 20 randomly sampled inputs (See 2.3.1). To have comparable results for each network, we trained the remaining models using the same seed that resulted in peak LSM accuracy. For NALSM, we used the same initialization and parameters for all networks and datasets. For LSM+AP-STDP, we hand-tuned STDP control parameters for each network and dataset combination to maximize validation accuracy (See Appendix A.6).

Sparse neuron-astrocyte connectivity We tested NALSM's accuracy as a function of neuron-astrocyte connection density on 3 best performing networks (per dataset). We trained NALSM with 10%, 20%, 40%, 60%, and 80% neuron-astrocyte density over 3 seeds for each of 3 networks. Regardless of connection sparseness, all IL/LL connections were modulated by A_{-}^{astro} (See 2.1)

NALSM with larger liquid sizes We tested NALSM performance for larger liquids. For each size, we trained 3 randomly generated networks, each on a random seed. All parameters and initialization were same as for $1,000$ neuron liquid. For maximum accuracy, we trained NALSM with an $8,000$ neuron liquid. For each dataset, we used 5 randomly generated networks trained on a random seed. Parameter $w_{astro} = 0.0075$ for both datasets. All other parameters and initialization were as before.

2.3.1 Branching factor of liquid

To evaluate a liquid's dynamics, we used the network branching factor, σ_{BF}, which quantifies network information flow amplification/decay. Liquid dynamics are sub-critical, near-critical and super-critical (chaotic) when $\sigma_{BF} < 1.0$, $\sigma_{BF} \approx 1.0$, and $\sigma_{BF} > 1.0$. We calculated σ_{BF} as done in [26], with offset $\phi = 0$ and time window $\Delta = 4\ ms$ as per [22].

3 Results

3.1 Baseline LSM performance

We established a benchmark accuracy for the baseline LSM on MNIST and N-MNIST datasets (See 2.3). We acquired our baseline by averaging over 10 randomly generated liquids with $1,000$ neurons (See 2.1). The LSM achieved a top accuracy of 95.44% ($95.30 \pm 0.11\%$) on MNIST, and 95.35% ($95.02 \pm 0.15\%$) on N-MNIST (See 2.2). For MNIST, this was comparable to the previously reported state-of-the-art LSM accuracy [57], using the same sized liquid. Further, LSM accuracy was very sensitive to the liquid's weight (Fig. 2 A).

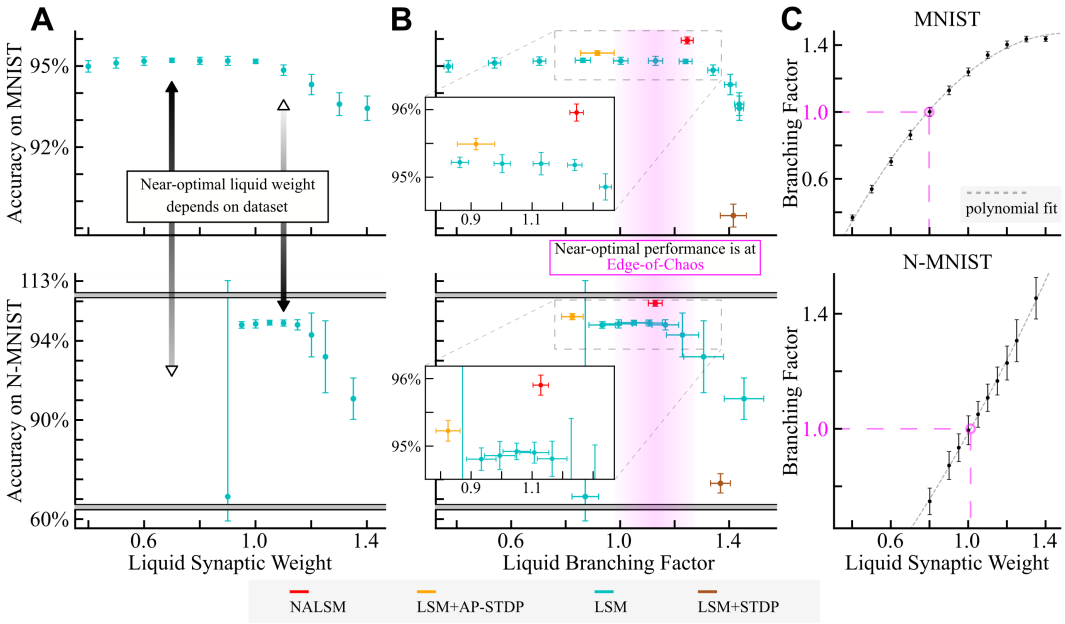

Figure 2: **LSM accuracy depends on liquid weight and dynamics.** (**A**) LSM accuracy shown as a function of its liquid weight, averaged over a set of 10 randomly generated networks for each dataset. (**B**) LSM accuracy shown with respect to liquid dynamics. For each weight, liquid dynamics were measured and averaged over all 10 networks. (**C**) Liquid dynamics shown with respect to liquid weight, averaged over all 10 networks. Error bars are standard deviation. See Appendix A.9 for polynomial fits.

3.2 LSM performance peaks at the edge-of-chaos

The peak LSM accuracy on each dataset corresponded to a different liquid synaptic weight. Specifically, there were cases where a liquid with weights tuned for maximum accuracy on MNIST, would catastrophically fail on N-MNIST (Fig. 2 A). Also, LSM accuracy on MNIST plateaued for a wider range of weights than on N-MNIST, which can be attributed to N-MNIST's greater difficulty caused by its variability over the temporal dimension (See Appendix A.1). Combined, this indicated that LSM training requires extensive hand-tuning of weights for each specific dataset.

Since edge-of-chaos dynamics are well known to result in near-maximum LSM performance [58, 19–21], dataset-specific hand-tuning can be significantly reduced by replacing accuracy with liquid dynamics as the target output of weight tuning. Indeed, LSM accuracy was near-maximum for both datasets, when the liquid's branching factor was in $1.0 - 1.2$ range, or at the edge-of-chaos (Fig. 2 B) (See 2.3.1). This agreed with studies showing that information transfer in finite sized systems peaks slightly in the super-critical phase [59]. Although each dataset still had different weight ranges correspond to the edge-of-chaos, the relationship between liquid dynamics and weight was positive for both datasets (Fig. 2 C). Known to generalize beyond specific datasets [20], this relationship suggested that edge-of-chaos dynamics can be organized using STDP, by providing it directional feedback from current liquid dynamics.

3.3 Astrocyte-modulated plasticity organizes edge-of-chaos dynamics in a liquid

The LIM astrocyte model stabilized liquid dynamics at the edge-of-chaos as we presented a continuous stream of samples to the neuron-astrocyte liquid (Fig. 2 B). Since the LIM astrocyte directly approximated liquid dynamics and, as feedback, directly controlled STDP depression learning rate (See 2.1), NALSM required no dataset-specific hand-tuning. As a result, we used the same weight intialization and parameters to benchmark NALSM on both MNIST and N-MNIST (See 2.3).

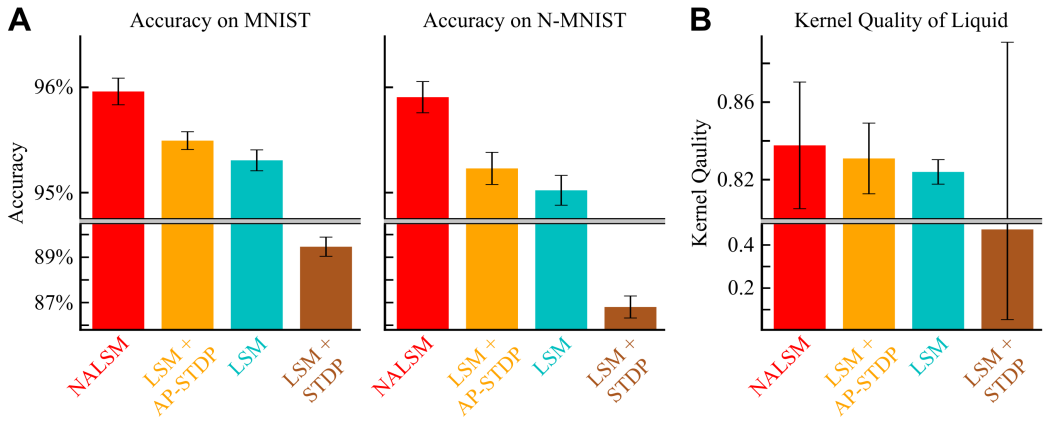

Figure 3: **Comparison of model accuracy and liquid computational capacity.** (**A**) Accuracy performance of the proposed NALSM model was compared, on MNIST and N-MNIST, against 3 related models: 1) the baseline LSM, 2) LSM with activity-based STDP (LSM+AP-STDP), and 3) LSM with unregulated STDP (LSM+STDP). For each dataset and model, accuracy was evaluated using 10 randomly generated networks, each of which was trained on a random seed. This set of 10 seeds was used for all models. (**B**) Computational capacity of each model was measured using a kernel quality metric that encompassed the linear separation and generalization capability of the liquid (See Section A.2) Error bars are standard deviation.

3.4 Benchmarking NALSM performance on MNIST and N-MNIST

On both datasets, NALSM achieved superior performance to comparable LSM models of the same size. Using $1,000$ liquid neurons, NALSM achieved a top accuracy of 96.15% ($95.96 \pm 0.13\%$) on MNIST and 96.13% ($95.90 \pm 0.16\%$) on N-MNIST; outperforming LSM model's top accuracy by 0.71% on MNIST and 0.78% on N-MNIST (Fig. 3 A). We also compared NALSM to a state-of-the-art LSM STDP method, AP-STDP (See 2.3). The LSM+AP-STDP model required more extensive dataset-specific hand-tuning than the baseline LSM due to its additional STDP control parameters (See Appendix A.6). Resulting in top accuracy of 95.62% ($95.49 \pm 0.09\%$) and 95.43% ($95.23 \pm 0.16\%$), the LSM+AP-STDP model was superseded by NALSM by 0.53% and 0.70% on MNIST and N-MNIST, respectively. As a control measure, we also trained a LSM with unregulated STDP (See 2.1). The LSM+STDP model significantly under-performed compared to all other models achieving a top accuracy of 90.52% ($89.47\% \pm 0.45$) on MNIST and 87.71% ($86.80\% \pm 0.51$) on N-MNIST. We attributed this under-performance to the LSM+STDP liquid's excessive chaotic dynamics (Fig. 2 B) which are well known to decrease liquid computational capacity [58, 59].

The NALSM had the most robust accuracy performance across the two datasets out of all the compared LSM models. With no dataset-specific tuning, NALSM's average accuracy on N-MNIST was lower than the accuracy on MNIST by only -0.05%. This was $5 - 50$ times less than for the LSM+AP-STDP (-0.26%), LSM (-0.29%), and LSM+STDP (-2.66%) models.

We attributed NALSM's performance advantage to the neuron-astrocyte liquid's near-proximity to the edge-of-chaos and improved computational capacity. For both datasets, the proposed NALSM achieved edge-of-chaos dynamics where baseline LSM performance peaked right before it started to decline with increasing chaos (Fig. 2 B). This suggested that NALSM's performance advantage, compared to a LSM with similarly critical dynamics, was due to the addition of astrocyte-modulated STDP (See 2.1, 2.2.1). While LSM+AP-STDP and LSM+STDP models also had STDP, their lower performance was explained by their sub-critical and super-critical dynamics, respectively (Fig. 2 B). We further confirmed that model performance was indeed dependent on the liquid's computational properties by measuring the liquid's kernel quality for each model. This encompassed both the linear separation and generalization capability of the liquid (See A.2). Higher model accuracy corresponded to higher kernel quality for all 4 models (Fig. 3 B). This indicated that NALSM's performance increase resulted from the improved computational properties and edge-of-chaos dynamics in its liquid.

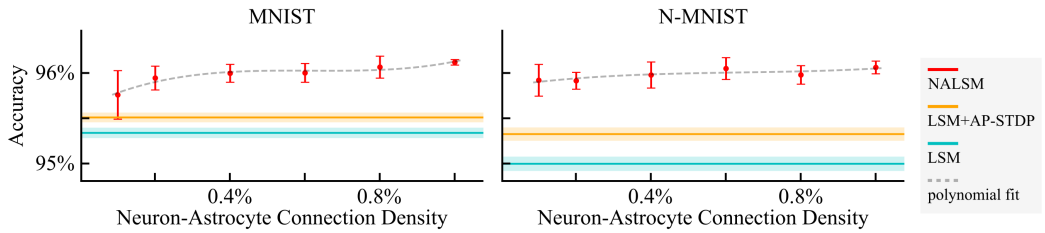

Figure 4: **NALSM maintains accuracy advantage with sparse neuron-astrocyte connectivity.** For MNIST and N-MNIST, NALSM accuracy was evaluated with respect to neuron-astrocyte connection density. For each density, NALSM performance was compared to LSM and LSM+AP-STDP average accuracy. NALSM data points are average values over 9 experiments (3 networks $\times$ 3 seeds). Error bars and shaded areas are standard deviation. See Appendix A.9 for polynomial fits.

3.5 NALSM maintains performance with sparse neuron-astrocyte connectivity

The NALSM maintained its accuracy advantage even with neuron-astrocyte connection densities as low as 10% (Fig. 4). In the brain, astrocytes contact only approximately 65% of all synapses in their surroundings [60]. We tested NALSM performance as function of neuron-astrocyte connection density. The NALSM mean accuracy decreased marginally with increasingly sparse connectivity, while variability in performance was minimal across densities. At 10% connectivity, average NALSM accuracy decreased by 0.36% for MNIST and 0.14% for N-MNIST compared to 100% connection density. In both cases, average NALSM accuracy was still above LSM and LSM+APSTDP average accuracy.

3.6 Larger liquids increase NALSM accuracy

The NALSM accuracy improved with increased liquid size, saturating at approximately $8,000$ neurons (See Appendix A.7). NALSM8000 achieved a top accuracy of 97.61% ($97.49 \pm 0.11\%$) on MNIST and 97.51% ($97.42 \pm 0.07\%$) on N-MNIST. Compared to previously reported benchmarks on MNIST, the NALSM8000 outperformed all brain-inspired learning methods that do not use backpropagation of gradients or its approximation through feedback alignment [61, 62], with the exception of [63]. While [63] demonstrated that a fully-connected 2-layer spiking network can achieve high accuracy through a combination of biologically-plausible plasticity rules, it is not clear how such an approach would scale to more layers without some form of backpropagation. Conversely, multi-layered LSMs have been shown to work without backpropagation [8, 10]. Further, NALSM8000 used approximately $1/3$ ($\approx 1,199,407 \pm 453$) of number of trainable(plastic) connections as in [63]. Compared to top accuracies reported for fully-connected multi-layered spiking neural networks trained with backpropagation, the NALSM8000 achieved comparable performance on both datasets; outperformning multiple reported results for each dataset (Table 1) (See Appendix A.8).

4 Discussion and Broader Impact

Ironically, LSMs are the most brain-like yet the most difficult to train learning models. Here, we proposed the astrocytic modulation of STDP as a method to integrate edge-of-chaos dynamics and STDP into a single liquid, thereby simultaneously improving LSM performance and decreasing data-specific tuning. We showed that the synergy of STDP and edge-of-chaos dynamics improved the computational capacity of the liquid, which translated to better than state-of-the-art LSM accuracy on MNIST and N-MNIST. Our results indicate that, given a large enough liquid, NALSM performance compares to current fully-connected multi-layer spiking neural networks trained via backpropagation.

The reported narrowing of the performance gap between brain-inspired LSM and deep networks suggests that studying the interaction among the brain's computational principles can help our learning models to reach human-like performance. Indeed, our results demonstrate that the synergy of brain-inspired astrocyte-modulated STDP and edge-of-chaos dynamics resulted in the superior performance of NALSM compared to 1) a LSM with edge-of-chaos dynamics but without STDP, and 2) a LSM with STDP, but without edge-of-chaos dynamics. Aligning with other studies showing that liquid topology impacts LSM accuracy [74], we also showed that a brain-inspired, sparse,

Table 1: Comparison to brain-inspired and fully-connected multi-layer spiking neural networks.

Model	Layers	Learning Method	Accuracy
Dataset: MNIST			
Unsupervised-SNN [64]	2	STDP	95%
Multi-liquid LSM [57]	2	GD on last layer	95.5%
NALSM1000	**2**	**astro-STDP, GD on last layer**	**96.15%**
LIF-BA [62]	3	Broadcast feedback alignment	97.09%
Temporal SNN [65]	2	Temporal backpropagation	97.2%
STiDi-BP [66]	2	Backpropagation	97.4%
NALSM8000	**2**	**astro-STDP, GD on last layer**	**97.61%**
SN [67]	3	Backpropagation	97.93%
GLSNN [61]	4	Global feedback alignment, STDP	98.62%
Balance-SNN [63]	2	Equi-prop, STDP, STP	98.64%
BPSNN [68]	3	Backpropagation	98.88%
STBP [69]	2	Spatial and temporal backpropagation	98.89%
Analogue MLP [70]	2	Backpropagation	98.4%
Dataset: N-MNIST			
DECOLLE [71]	3	Backpropagation	96%
NALSM1000	**2**	**astro-STDP, GD on last layer**	**96.13%**
AER-SNN [72]	2	Backpropagation	96.3%
NALSM8000	**2**	**astro-STDP, GD on last layer**	**97.51%**
BPSNN [68]	3	Backpropagation	98.74%
STBP [69]	2	Spatial and temporal backpropagation	98.78%
SLAYER [73]	3	Backpropagation	98.89%

*GD: gradient descent

3D-distance-based network architecture can improve the computational capacity of a single liquid. Specifically, our baseline 3D LSM achieved comparable accuracy to the multi-liquid LSM [57], which improved performance of a single dimensionless liquid by partitioning it into multiple liquids.

Here, we introduced astrocytes as a second processing unit to neuromorphic computing. Our results help to dismantle a dogma that "brain = neurons" and clear up the 100-years old "neuron doctrine", that the neuron is the *only* processing unit in the brain [75–77]. Adding an orthogonal dimension to neuronal processing, with distinct temporal and spatial characteristics [52, 53], we demonstrated the positive contribution of astrocyte-modulated STDP to the computational capacity of the LSM liquid. This offers a natural extension of learning beyond synapses through semi-local unsupervised plasticity mechanisms that can be fine-tuned to trade-off computation complexity versus accuracy. In addition, our results are not limited to the gradient descent trained linear output used in this work, which can be replaced by several other single-layer spiking networks [78–80], making our method directly compatible with current neuromorphic hardware [81]. The asynchronous neuronal computation and the low temporal and spatial dimension that astrocytes add to LSM training and inference may further reduce energy consumption and memory requirements compared to current LSM solutions.

Our work shows how recent insights on the brain's neurophysiology from cellular neuroscience can be synthesized with neuromorphic computing, directly leading to new and improved intelligent systems, and in time significantly influencing artificial intelligence research, while also extending the computational understanding of brain function and dysfunction. Indeed, in the neuromorphic computing paradigm, neuroscience has been regarded as the bearer of truth. Underappreciated for over a century, astrocytes have been absent from both prevailing computational hypotheses on how the brain learns, and from subsequent efforts to translate that knowledge into efficient models of intelligence. Our paper tackles these two shortcomings. The first problem is mitigated by computational modeling, that maps cellular principles onto network behavior. The second problem is addressed by demonstrating the computational advantages of astrocyte neuromodulation.

By showing how computational capacity can be maximized at the edge-of-chaos, we aimed to broaden the applicability of LSM to complex spatio-temporal problems that require integration of data over multiple sources and time-scales, making LSMs suitable for real-life applications of edge computing. Our so far results suggest that this is a direction worth pursuing.

References

[1] Jack D. Kendall and Suhas Kumar. The building blocks of a brain-inspired computer. *Applied Physics Reviews*, 7(1):011305, 2020. doi: 10.1063/1.5129306.

[2] Guangzhi Tang, Neelesh Kumar, and Konstantinos P. Michmizos. Reinforcement co-learning of deep and spiking neural networks for energy-efficient mapless navigation with neuromorphic hardware. In *2020 IEEE/RSJ International Conference on Intelligent Robots and Systems (IROS)*, pages 6090–6097, 2020. doi: 10.1109/IROS45743.2020.9340948.

[3] Mike Davies, Narayan Srinivasa, Tsung-Han Lin, Gautham Chinya, Yongqiang Cao, Sri Harsha Choday, Georgios Dimou, Prasad Joshi, Nabil Imam, Shweta Jain, Yuyun Liao, Chit-Kwan Lin, Andrew Lines, Ruokun Liu, Deepak Mathaikutty, Steven McCoy, Arnab Paul, Jonathan Tse, Guruguhanathan Venkataramanan, Yi-Hsin Weng, Andreas Wild, Yoonseok Yang, and Hong Wang. Loihi: A neuromorphic manycore processor with on-chip learning. *IEEE Micro*, 38(1): 82–99, 2018. doi: 10.1109/MM.2018.112130359.

[4] Guangzhi Tang, Arpit Shah, and Konstantinos P. Michmizos. Spiking neural network on neuromorphic hardware for energy-efficient unidimensional slam. In *2019 IEEE/RSJ International Conference on Intelligent Robots and Systems (IROS)*, pages 4176–4181, 2019. doi: 10.1109/IROS40897.2019.8967864.

[5] Keyan Cao, Yefan Liu, Gongjie Meng, and Qimeng Sun. An overview on edge computing research. *IEEE Access*, 8:85714–85728, 2020. doi: 10.1109/ACCESS.2020.2991734.

[6] Jiasi Chen and Xukan Ran. Deep learning with edge computing: A review. *Proceedings of the IEEE*, 107(8):1655–1674, 2019. doi: 10.1109/JPROC.2019.2921977.

[7] Wolfgang Maass, Thomas Natschläger, and Henry Markram. Real-time computing without stable states: A new framework for neural computation based on perturbations. *Neural Computation*, 14(11):2531–2560, 2002. doi: 10.1162/089976602760407955.

[8] Kudithipudi Dhireesha Soures Nicholas. Deep liquid state machines with neural plasticity for video activity recognition. *Frontiers in Neuroscience*, 13:686, 2019. doi: 10.3389/fnins.2019.00686.

[9] Wachirawit Ponghiran, Gopalakrishnan Srinivasan, and Kaushik Roy. Reinforcement learning with low-complexity liquid state machines. *Frontiers in Neuroscience*, 13:883, 2019. ISSN 1662-453X. doi: 10.3389/fnins.2019.00883.

[10] Qian Wang and Peng Li. D-lsm: Deep liquid state machine with unsupervised recurrent reservoir tuning. In *2016 23rd International Conference on Pattern Recognition (ICPR)*, pages 2652–2657, 2016. doi: 10.1109/ICPR.2016.7900035.

[11] Shiya Liu, Lingjia Liu, and Yang Yi. Quantized reservoir computing on edge devices for communication applications. In *2020 IEEE/ACM Symposium on Edge Computing (SEC)*, pages 445–449, 2020. doi: 10.1109/SEC50012.2020.00068.

[12] Shiming Li, Lei Wang, Shiying Wang, and Weixia Xu. Liquid state machine applications mapping for noc-based neuromorphic platforms. In Dezun Dong, Xiaoli Gong, Cunlu Li, Dongsheng Li, and Junjie Wu, editors, *Advanced Computer Architecture*, pages 277–289, Singapore, 2020. Springer Singapore. ISBN 978-981-15-8135-9.

[13] Bon Woong Ku, Yu Liu, Yingyezhe Jin, Sandeep Samal, Peng Li, and Sung Kyu Lim. Design and architectural co-optimization of monolithic 3d liquid state machine-based neuromorphic processor. In *2018 55th ACM/ESDA/IEEE Design Automation Conference (DAC)*, pages 1–6, 2018. doi: 10.1109/DAC.2018.8465837.

[14] Josep L. Rosselló, Miquel L. Alomar, Antoni Morro, Antoni Oliver, and Vincent Canals. High-density liquid-state machine circuitry for time-series forecasting. *International Journal of Neural Systems*, 26(05):1550036, 2016. doi: 10.1142/S0129065715500367. PMID: 26906454.

[15] Ismael Balafrej and Jean Rouat. P-critical: A reservoir autoregulation plasticity rule for neuromorphic hardware, 2020.

[16] Simon Brodeur and Jean Rouat. Regulation toward self-organized criticality in a recurrent spiking neural reservoir. In Alessandro E. P. Villa, Włodzisław Duch, Péter Érdi, Francesco Masulli, and Günther Palm, editors, *Artificial Neural Networks and Machine Learning – ICANN 2012*, pages 547–554, Berlin, Heidelberg, 2012. Springer Berlin Heidelberg.

[17] Yingyezhe Jin and Peng Li. Ap-stdp: A novel self-organizing mechanism for efficient reservoir computing. In *2016 International Joint Conference on Neural Networks (IJCNN)*, pages 1158–1165, 2016. doi: 10.1109/IJCNN.2016.7727328.

[18] D. Norton and D. Ventura. Preparing more effective liquid state machines using hebbian learning. In *The 2006 IEEE International Joint Conference on Neural Network Proceedings*, pages 4243–4248, 2006. doi: 10.1109/IJCNN.2006.246996.

[19] Robert Legenstein and Wolfgang Maass. Edge of chaos and prediction of computational performance for neural circuit models. *Neural Networks*, 20(3):323 – 334, 2007. ISSN 0893-6080. doi: 10.1016/j.neunet.2007.04.017. Echo State Networks and Liquid State Machines.

[20] Nils Bertschinger and Thomas Natschläger. Real-time computation at the edge of chaos in recurrent neural networks. *Neural Computation*, 16(7):1413–1436, 2004. doi: 10.1162/089976604323057443.

[21] Chris G. Langton. Computation at the edge of chaos: phase transitions and emergent computation. *Physica D: Nonlinear Phenomena*, 42(1):12 – 37, 1990. ISSN 0167-2789. doi: 10.1016/0167-2789(90)90064-V.

[22] John M. Beggs and Dietmar Plenz. Neuronal avalanches in neocortical circuits. *Journal of Neuroscience*, 23(35):11167–11177, 2003. ISSN 0270-6474. doi: 10.1523/JNEUROSCI.23-35-11167.2003.

[23] Oren Shriki, Jeff Alstott, Frederick Carver, Tom Holroyd, Richard N.A. Henson, Marie L. Smith, Richard Coppola, Edward Bullmore, and Dietmar Plenz. Neuronal avalanches in the resting meg of the human brain. *Journal of Neuroscience*, 33(16):7079–7090, 2013. ISSN 0270-6474. doi: 10.1523/JNEUROSCI.4286-12.2013.

[24] Dante R. Chialvo. Emergent complex neural dynamics. *Nature Physics*, 6:744–750, 2010. ISSN 1745-2481. doi: 10.1038/nphys1803.

[25] Daniel E. Feldman. Synaptic mechanisms for plasticity in neocortex. *Annual Review of Neuroscience*, 32(1):33–55, 2009. doi: 10.1146/annurev.neuro.051508.135516. PMID: 19400721.

[26] Nigel Stepp, Dietmar Plenz, and Narayan Srinivasa. Synaptic plasticity enables adaptive self-tuning critical networks. *PLOS Computational Biology*, 11(1):1–28, 01 2015. doi: 10.1371/journal.pcbi.1004043.

[27] Friedemann Zenke and Wulfram Gerstner. Hebbian plasticity requires compensatory processes on multiple timescales. *Philosophical Transactions of the Royal Society B: Biological Sciences*, 372(1715):20160259, 2017. doi: 10.1098/rstb.2016.0259.

[28] Alanna Watt and Niraj Desai. Homeostatic plasticity and stdp: keeping a neuron's cool in a fluctuating world. *Frontiers in Synaptic Neuroscience*, 2:5, 2010. ISSN 1663-3563. doi: 10.3389/fnsyn.2010.00005.

[29] L. F. Abbott and Sacha B. Nelson. Synaptic plasticity: taming the beast. *Nature Neuroscience*, 3(11):1178–1183, 2000. ISSN 1546-1726. doi: 10.1038/81453.

[30] Gertrudis Perea and Alfonso Araque. Glia modulates synaptic transmission. *Brain Research Reviews*, 63(1):93–102, 2010. ISSN 0165-0173.

[31] Xiaoning Han, Michael Chen, Fushun Wang, Martha Windrem, Su Wang, Steven Shanz, Qiwu Xu, Nancy Ann Oberheim, Lane Bekar, and Sarah Betstadt. Forebrain engraftment by human glial progenitor cells enhances synaptic plasticity and learning in adult mice. *Cell Stem Cell*, 12(3):342–353, 2013. ISSN 1934-5909.

[32] Shivendra Tewari and Vladimir Parpura. A possible role of astrocytes in contextual memory retrieval: An analysis obtained using a quantitative framework. *Frontiers in Computational Neuroscience*, 7:145, 2013. ISSN 1662-5188. doi: 10.3389/fncom.2013.00145.

[33] Marta Navarrete and Alfonso Araque. Endocannabinoids potentiate synaptic transmission through stimulation of astrocytes. *Neuron*, 68(1):113–126, 2010. ISSN 0896-6273.

[34] Adar Adamsky, Adi Kol, Tirzah Kreisel, Adi Doron, Nofar Ozeri-Engelhard, Talia Melcer, Ron Refaeli, Henrike Horn, Limor Regev, and Maya Groysman. Astrocytic activation generates de novo neuronal potentiation and memory enhancement. *Cell*, 174(1):59–71. e14, 2018. ISSN 0092-8674.

[35] Francesco Petrelli, Glenn Dallérac, Luca Pucci, Corrado Calì, Tamara Zehnder, Sébastien Sultan, Salvatore Lecca, Andrea Chicca, Andrei Ivanov, Cédric S. Asensio, Vidar Gundersen, Nicolas Toni, Graham William Knott, Fulvio Magara, Jürg Gertsch, Frank Kirchhoff, Nicole Déglon, Bruno Giros, Robert H. Edwards, Jean-Pierre Mothet, and Paola Bezzi. Dysfunction of homeostatic control of dopamine by astrocytes in the developing prefrontal cortex leads to cognitive impairments. *Molecular Psychiatry*, 25(4):732–749, 2020. doi: 10.1038/s41380-018-0226-y.

[36] Tiina Manninen, Ausra Saudargiene, and Marja-Leena Linne. Astrocyte-mediated spike-timing-dependent long-term depression modulates synaptic properties in the developing cortex. *PLOS Computational Biology*, 16(11):1–29, 11 2020. doi: 10.1371/journal.pcbi.1008360.

[37] Jérémie Sibille, Ulrike Pannasch, and Nathalie Rouach. Astroglial potassium clearance contributes to short-term plasticity of synaptically evoked currents at the tripartite synapse. *The Journal of Physiology*, 592(1):87–102, 2014. doi: 10.1113/jphysiol.2013.261735.

[38] Rogier Min and Thomas Nevian. Astrocyte signaling controls spike timing–dependent depression at neocortical synapses. *Nature Neuroscience*, 15(5):746–753, 2012. doi: 10.1038/nn.3075.

[39] Alexander Stanley Thrane, Vinita Rangroo Thrane, Douglas Zeppenfeld, Nanhong Lou, Qiwu Xu, Erlend Arnulf Nagelhus, and Maiken Nedergaard. General anesthesia selectively disrupts astrocyte calcium signaling in the awake mouse cortex. *Proceedings of the National Academy of Sciences*, 109(46):18974–18979, 2012. ISSN 0027-8424. doi: 10.1073/pnas.1209448109.

[40] Jeannine Foley, Tamara Blutstein, SoYoung Lee, Christophe Erneux, Michael M. Halassa, and Philip Haydon. Astrocytic ip3/ca2+ signaling modulates theta rhythm and rem sleep. *Frontiers in Neural Circuits*, 11:3, 2017. ISSN 1662-5110. doi: 10.3389/fncir.2017.00003.

[41] Laura Bojarskaite, Daniel M. Bjørnstad, Klas H. Pettersen, Céline Cunen, Gudmund Horn Hermansen, Knut Sindre Åbjørsbråten, Rolf Sprengel, Koen Vervaeke, Wannan Tang, Rune Enger, and Erlend A. Nagelhus. Astrocytic ca2+ signaling is reduced during sleep and is involved in the regulation of slow wave sleep. *Nature Communications*, 11:3240, 2020. ISSN 2041-1723. doi: 10.1038/s41467-020-17062-2.

[42] Ashley M. Ingiosi, Christopher R. Hayworth, Daniel O. Harvey, Kristan G. Singletary, Michael J. Rempe, Jonathan P. Wisor, and Marcos G. Frank. A role for astroglial calcium in mammalian sleep and sleep regulation. *Current Biology*, 30:4373–4383.e7, 2020. doi: 10.1016/j.cub.2020.08.052.

[43] Enzo Tagliazucchi, Dante R. Chialvo, Michael Siniatchkin, Enrico Amico, Jean-Francois Brichant, Vincent Bonhomme, Quentin Noirhomme, Helmut Laufs, and Steven Laureys. Large-scale signatures of unconsciousness are consistent with a departure from critical dynamics. *Journal of The Royal Society Interface*, 13(114):20151027, 2016. doi: 10.1098/rsif.2015.1027.

[44] Timothy Bellay, Andreas Klaus, Saurav Seshadri, and Dietmar Plenz. Irregular spiking of pyramidal neurons organizes as scale-invariant neuronal avalanches in the awake state. *eLife*, 4: e07224, jul 2015. ISSN 2050-084X. doi: 10.7554/eLife.07224.

[45] Gerald Hahn, Adrian Ponce-Alvarez, Cyril Monier, Giacomo Benvenuti, Arvind Kumar, Frédéric Chavane, Gustavo Deco, and Yves Frégnac. Spontaneous cortical activity is transiently poised close to criticality. *PLOS Computational Biology*, 13(5):1–29, 05 2017. doi: 10.1371/journal.pcbi.1005543.

[46] Viola Priesemann, Mario Valderrama, Michael Wibral, and Michel Le Van Quyen. Neuronal avalanches differ from wakefulness to deep sleep – evidence from intracranial depth recordings in humans. *PLOS Computational Biology*, 9(3):1–14, 03 2013. doi: 10.1371/journal.pcbi.1002985.

[47] Erik D. Fagerholm, Romy Lorenz, Gregory Scott, Martin Dinov, Peter J. Hellyer, Nazanin Mirzaei, Clare Leeson, David W. Carmichael, David J. Sharp, Woodrow L. Shew, and Robert Leech. Cascades and cognitive state: focused attention incurs subcritical dynamics. *Journal of Neuroscience*, 35(11):4626–4634, 2015. ISSN 0270-6474. doi: 10.1523/JNEUROSCI.3694-14.2015.

[48] Vladimir Parpura and Philip G. Haydon. Physiological astrocytic calcium levels stimulate glutamate release to modulate adjacent neurons. *Proceedings of the National Academy of Sciences*, 97(15):8629–8634, 2000. ISSN 0027-8424. doi: 10.1073/pnas.97.15.8629.

[49] Catherine A. Christian and John R. Huguenard. Astrocytes potentiate gabaergic transmission in the thalamic reticular nucleus via endozepine signaling. *Proceedings of the National Academy of Sciences*, 110(50):20278–20283, 2013. doi: 10.1073/pnas.1318031110.

[50] Sara Mederos, Candela González-Arias, and Gertrudis Perea. Astrocyte–neuron networks: a multilane highway of signaling for homeostatic brain function. *Frontiers in Synaptic Neuroscience*, 10(45), 2018. ISSN 1663-3563. doi: 10.3389/fnsyn.2018.00045.

[51] Eiji Shigetomi, Sandip Patel, and Baljit S. Khakh. Probing the complexities of astrocyte calcium signaling. *Trends in Cell Biology*, 26(4):300–312, 2016. ISSN 0962-8924.

[52] Gertrudis Perea, Mriganka Sur, and Alfonso Araque. Neuron-glia networks: integral gear of brain function. *Frontiers in Cellular Neuroscience*, 8(378), 2014. ISSN 1662-5102. doi: 10.3389/fncel.2014.00378.

[53] Alfonso Araque, Giorgio Carmignoto, Philip G Haydon, Stéphane HR Oliet, Richard Robitaille, and Andrea Volterra. Gliotransmitters travel in time and space. *Neuron*, 81(4):728–739, 2014. ISSN 0896-6273.

[54] Y. Lecun, L. Bottou, Y. Bengio, and P. Haffner. Gradient-based learning applied to document recognition. *Proceedings of the IEEE*, 86(11):2278–2324, 1998. doi: 10.1109/5.726791.

[55] Garrick Orchard, Ajinkya Jayawant, Gregory K. Cohen, and Nitish Thakor. Converting static image datasets to spiking neuromorphic datasets using saccades. *Frontiers in Neuroscience*, 9:437, 2015. ISSN 1662-453X. doi: 10.3389/fnins.2015.00437.

[56] Abigail Morrison, Markus Diesmann, and Wulfram Gerstner. Phenomenological models of synaptic plasticity based on spike timing. *Biological Cybernetics*, 98(6):459–478, 2008. ISSN 1432-0770. doi: 10.1007/s00422-008-0233-1.

[57] Parami Wijesinghe, Gopalakrishnan Srinivasan, Priyadarshini Panda, and Kaushik Roy. Analysis of liquid ensembles for enhancing the performance and accuracy of liquid state machines. *Frontiers in Neuroscience*, 13:504, 2019. ISSN 1662-453X. doi: 10.3389/fnins.2019.00504.

[58] Joschka Boedecker, Oliver Obst, Joseph T Lizier, N Michael Mayer, and Minoru Asada. Information processing in echo state networks at the edge of chaos. *Theory Biosci.*, 131(3):205–13, 2012. doi: 10.1007/s12064-011-0146-8.

[59] Andre S. Ribeiro, Stuart A. Kauffman, Jason Lloyd-Price, Björn Samuelsson, and Joshua E. S. Socolar. Mutual information in random boolean models of regulatory networks. *Phys. Rev. E*, 77:011901, Jan 2008. doi: 10.1103/PhysRevE.77.011901.

[60] Bin Zhou, Yun-Xia Zuo, and Ruo-Tian Jiang. Astrocyte morphology: diversity, plasticity, and role in neurological diseases. *CNS Neuroscience & Therapeutics*, 25(6):665–673, 2019. doi: 10.1111/cns.13123.

[61] Dongcheng Zhao, Yi Zeng, Tielin Zhang, Mengting Shi, and Fei fei Zhao. Glsnn: A multi-layer spiking neural network based on global feedback alignment and local stdp plasticity. *Frontiers in Computational Neuroscience*, 14, 2020.

[62] Arash Samadi, T. Lillicrap, and D. Tweed. Deep learning with dynamic spiking neurons and fixed feedback weights. *Neural Computation*, 29:578–602, 2017.

[63] Tielin Zhang, Yi Zeng, Dongcheng Zhao, and Bo Xu. Brain-inspired balanced tuning for spiking neural networks. In *Proceedings of the Twenty-Seventh International Joint Conference on Artificial Intelligence, IJCAI-18*, pages 1653–1659. International Joint Conferences on Artificial Intelligence Organization, 7 2018. doi: 10.24963/ijcai.2018/229. URL `https://doi.org/10.24963/ijcai.2018/229`.

[64] Peter Diehl and Matthew Cook. Unsupervised learning of digit recognition using spike-timing-dependent plasticity. *Frontiers in Computational Neuroscience*, 9:99, 2015. ISSN 1662-5188. doi: 10.3389/fncom.2015.00099.

[65] Hesham Mostafa. Supervised learning based on temporal coding in spiking neural networks. *IEEE Transactions on Neural Networks and Learning Systems*, 29:3227–3235, 2018.

[66] Maryam Mirsadeghi, Majid Shalchian, Saeed Reza Kheradpisheh, and Timothée Masquelier. Stidi-bp: Spike time displacement based error backpropagation in multilayer spiking neural networks. *Neurocomputing*, 427:131–140, 2021. ISSN 0925-2312. doi: https://doi.org/10.1016/j.neucom.2020.11.052.

[67] Peter O'Connor and M. Welling. Deep spiking networks. *ArXiv*, abs/1602.08323, 2016.

[68] Jun Haeng Lee, Tobi Delbruck, and Michael Pfeiffer. Training deep spiking neural networks using backpropagation. *Frontiers in Neuroscience*, 10:508, 2016. ISSN 1662-453X. doi: 10.3389/fnins.2016.00508.

[69] Yujie Wu, Lei Deng, Guoqi Li, Jun Zhu, and Luping Shi. Spatio-temporal backpropagation for training high-performance spiking neural networks. *Frontiers in Neuroscience*, 12:331, 2018. ISSN 1662-453X. doi: 10.3389/fnins.2018.00331.

[70] P.Y. Simard, D. Steinkraus, and J.C. Platt. Best practices for convolutional neural networks applied to visual document analysis. In *Seventh International Conference on Document Analysis and Recognition, 2003. Proceedings.*, pages 958–963, 2003. doi: 10.1109/ICDAR.2003.1227801.

[71] Jacques Kaiser, Hesham Mostafa, and Emre Neftci. Synaptic plasticity dynamics for deep continuous local learning (decolle). *Frontiers in Neuroscience*, 14:424, 2020. ISSN 1662-453X. doi: 10.3389/fnins.2020.00424.

[72] Qianhui Liu, Haibo Ruan, Dong Xing, H. Tang, and Gang Pan. Effective aer object classification using segmented probability-maximization learning in spiking neural networks. In *AAAI*, 2020.

[73] S. Shrestha and G. Orchard. Slayer: Spike layer error reassignment in time. In *NeurIPS*, 2018.

[74] Han Ju, Jian-Xin Xu, Edmund Chong, and Antonius M.J. VanDongen. Effects of synaptic connectivity on liquid state machine performance. *Neural Networks*, 38:39–51, 2013. ISSN 0893-6080. doi: https://doi.org/10.1016/j.neunet.2012.11.003.

[75] Michael M. Halassa and Philip G. Haydon. Integrated brain circuits: astrocytic networks modulate neuronal activity and behavior. *Annual Review of Physiology*, 72(1):335–355, 2010. doi: 10.1146/annurev-physiol-021909-135843.

[76] Eduardo E. Benarroch. Neuron-astrocyte interactions: partnership for normal function and disease in the central nervous system. *Mayo Clinic Proceedings*, 80(10):1326–1338, 2005. ISSN 0025-6196.

[77] Dionysia T. Theodosis, Dominique A. Poulain, and Stéphane H. R. Oliet. Activity-dependent structural and functional plasticity of astrocyte-neuron interactions. *Physiological Reviews*, 88(3):983–1008, 2008. doi: 10.1152/physrev.00036.2007.

[78] Filip Ponulak and Andrzej Kasiński. Supervised learning in spiking neural networks with resume: Sequence learning, classification, and spike shifting. *Neural Comput.*, 22(2):467–510, February 2010. ISSN 0899-7667. doi: 10.1162/neco.2009.11-08-901.

[79] Robert Urbanczik and Walter Senn. A Gradient Learning Rule for the Tempotron. *Neural Computation*, 21(2):340–352, 02 2009. ISSN 0899-7667. doi: 10.1162/neco.2008.09-07-605.

[80] Robert Gütig and Haim Sompolinsky. The tempotron: a neuron that learns spike timing–based decisions. *Nature Neuroscience*, 9(3):420–428, 2006. doi: 10.1038/nn1643.

[81] Guangzhi Tang, Ioannis E. Polykretis, Vladimir A. Ivanov, Arpit Shah, and Konstantinos P. Michmizos. Introducing astrocytes on a neuromorphic processor: Synchronization, local plasticity and edge of chaos. *ACM Proceedings of 2019 Neuroinspired Computing Elements (NICE 2019)*, 1(1):1–10, 2019. doi: arXiv:1907.01620.

[82] Wolfgang Maass, Robert Legenstein, and Nils Bertschinger. Methods for estimating the computational power and generalization capability of neural microcircuits. In *Proceedings of the 17th International Conference on Neural Information Processing Systems*, NIPS'04, page 865–872, Cambridge, MA, USA, 2004. MIT Press.

Checklist

1. For all authors...
   (a) Do the main claims made in the abstract and introduction accurately reflect the paper's contributions and scope? [Yes]
   (b) Did you describe the limitations of your work? [No]
   (c) Did you discuss any potential negative societal impacts of your work? [No] The field is still not at the stage of deploying on real world applications.
   (d) Have you read the ethics review guidelines and ensured that your paper conforms to them? [Yes]
2. If you are including theoretical results...
   (a) Did you state the full set of assumptions of all theoretical results? [N/A]
   (b) Did you include complete proofs of all theoretical results? [N/A]
3. If you ran experiments...
   (a) Did you include the code, data, and instructions needed to reproduce the main experimental results (either in the supplemental material or as a URL)? [Yes] We provide all data (as excel file and appendix) and provide code with instructions to reproduce results.
   (b) Did you specify all the training details (e.g., data splits, hyperparameters, how they were chosen)? [Yes] Yes, all details are in section 2 or in the the appendix.
   (c) Did you report error bars (e.g., with respect to the random seed after running experiments multiple times)? [Yes]
   (d) Did you include the total amount of compute and the type of resources used (e.g., type of GPUs, internal cluster, or cloud provider)? [Yes] This is included in the appendix
4. If you are using existing assets (e.g., code, data, models) or curating/releasing new assets...
   (a) If your work uses existing assets, did you cite the creators? [Yes] In section 2
   (b) Did you mention the license of the assets? [N/A]
   (c) Did you include any new assets either in the supplemental material or as a URL? [Yes]
   (d) Did you discuss whether and how consent was obtained from people whose data you're using/curating? [N/A]
   (e) Did you discuss whether the data you are using/curating contains personally identifiable information or offensive content? [N/A]
5. If you used crowdsourcing or conducted research with human subjects...
   (a) Did you include the full text of instructions given to participants and screenshots, if applicable? [N/A]
   (b) Did you describe any potential participant risks, with links to Institutional Review Board (IRB) approvals, if applicable? [N/A]
   (c) Did you include the estimated hourly wage paid to participants and the total amount spent on participant compensation? [N/A]